Paste 2026 – AB Fourie, M Horta, M Oliveira & S Wilson (eds)

doi:10.36487/ACG_repo/2655_10

Hydraulic fracturing as a novel technique for strength evaluation of cemented paste backfill: influence of injection flow rate on fracture initiation pressure

James Frimpong [a], Rohit Pandey [a,*]

[a] *Department of Mining and Mineral Engineering, Virginia Tech, USA*

Abstract

Cemented paste backfill (CPB) is a critical ground control material in underground mining to provide support and stability to mined-out voids, and accurate strength assessment is essential for ensuring long-term stability and safety. Conventional strength evaluation methods, such as uniaxial compressive strength tests on surface-cured specimens, often fail to represent actual in situ conditions, leading to unreliable strength estimates. To overcome this limitation, a new laboratory technique based on hydraulic fracturing has been developed to directly evaluate CPB strength under in situ conditions. The method determines the fracture initiation pressure (FIP), the maximum pressure at which the backfill first fractures, which has been verified as a reliable indicator of CPB strength. This study focuses on investigating the role of injection flow rate in hydraulic fracturing tests as part of validating the technique. Cylindrical CPB samples were fractured using AW32 hydraulic oil at controlled flow rates ranging from 1 to 50 ml/min. Results show that flow rate influences fracture initiation at lower rates (1–8 ml/min). At these low rates, gradual fluid delivery causes slower pressurisation, increased fluid leak-off, and delayed fracture onset, resulting in reduced FIP values. As flow rate increases, FIP rises, reflecting more efficient pressurisation and reduced leak-off. However, beyond 8 ml/min, the influence of flow rate diminishes, and the inherent variability in sample strength becomes more significant than the variations in FIP caused by changes in flow rate. The findings highlight that flow rate is a critical parameter to consider when applying hydraulic fracturing for CPB testing. Practically, this study establishes a baseline recommendation: low flow rates are unsuitable for strength estimation. To obtain the most representative FIP-based strength index, higher injection flow rate should be used, where rate effects diminish and variability in FIP is dominated by material properties. These outcomes provide a strong foundation for advancing hydraulic fracturing as a reliable method for CPB strength assessment.

Keywords: *cemented paste backfill, hydraulic fracturing, fracture initiation pressure, injection flow rate, strength assessment, ground control*

1 Introduction

1.1 Background

Cemented paste backfill (CPB) is an engineered material placed in mined-out stopes and drifts to restore ground stability and ensure safe mining operations underground (Kesimal et al. 2005; Li et al. 2017; Wang et al. 2020; Yilmaz 2010). It is typically composed of dewatered mill tailings, water, and a cementitious binder such as Portland cement or blended alternatives, which are mixed at surface backfill plants and then transported underground through gravity-fed or pumped pipeline systems (Chen et al. 2022; Qiu et al. 2020; Xin 2021). By utilising mine tailings as a primary ingredient, CPB not only provides structural support but also

* Corresponding author. Email address: rpandey@vt.edu

reduces the volume of tailings requiring surface storage, thereby lowering the environmental risks associated with conventional tailings storage facilities when appropriately managed (Sheshpari 2015; Yin et al. 2020).

The in situ strength and performance of CPB are critical considerations in underground mine planning, as they directly influence ground stability, operational safety, and productivity. Strength assessment at different curing stages, particularly the early and late phases, is essential to ensure the backfill performs as intended. Early-age strength is vital to guarantee that freshly placed CPB can sustain its own weight and remain stable without relying on the bulkhead for support. Mining personnel and equipment are only permitted near the fill area once the CPB can self-support, reducing risks associated with potential bulkhead failures, a hazard documented in several mining operations (Helinski 2007; Yumlu & Guresci 2007). Conversely, late-age strength evaluation is essential for ensuring long-term structural competence of the backfill. Adequate cured strength prevents uncontrolled ground movement and enables safe extraction of adjacent or underlying stopes and drifts, facilitating efficient and continuous mining operations (Mitchell 1991). Despite its importance, in situ backfill strength is rarely measured in current industry practice, leaving critical design decisions to indirect indicators or conservative estimates.

Current industry practice for evaluating the strength of CPB involves preparing cylindrical specimens at the surface paste plant and curing them under controlled laboratory conditions. These samples are later tested in uniaxial compression at predefined curing intervals to estimate backfill strength. However, this approach poorly represents the actual in situ curing environment, leading to substantial variability in results often with coefficients of variation ranging from 15–60%, compared with only 3–6% typically observed in the concrete industry. This elevated variability is driven largely by the inherent heterogeneity of mine tailings and binder–tailings interactions, rather than limitations of the uniaxial compressive strength (UCS) testing methodology itself (Stone 2021). When direct assessment of in situ strength becomes necessary, alternative field methods such as cone penetration testing, self-boring pressuremeter testing, or core extraction from placed fill are employed (Aref 1988; Been et al. 2002; Johnson et al. 2015; Le Roux et al. 2002, 2005). Each, however, presents significant operational and technical challenges. In situ coring is often attempted when more representative strength data are required, but due to the relatively low strength and brittle nature of CPB, the material commonly fails during drilling, making recovery of intact cores extremely difficult (Le Roux et al. 2002).

To overcome this limitation, a hydraulic-fracturing-based testing technique was recently introduced (Frimpong & Pandey 2025; Frimpong et al. 2025). In this approach, controlled pressurisation of a small borehole within a CPB specimen produces a localised tensile fracture, and the fracture initiation pressure (FIP), the peak pressure recorded at the onset of cracking, is interpreted as an index of the material's tensile strength. Laboratory validation has demonstrated that FIP correlates strongly with benchmark strength parameters such as UCS, Brazilian tensile strength (BTS), Mode-I fracture toughness (K_{Ic}), establishing hydraulic fracturing as a viable, direct measure of CPB strength. Although the FIP-based technique marks a significant advancement, its broader application requires a clear understanding of how testing parameters affect the measured response. Among these parameters, the injection flow rate plays a particularly important role.

Hydraulic fracturing has long been recognised as an effective tool for characterising the mechanical response of brittle and weakly cemented materials under tensile loading. Classical studies such as Hubbert & Willis (1957) and Haimson & Fairhurst (1967, 1969) established the theoretical basis for breakdown pressure in impermeable and permeable rocks, emphasising the competing roles of pore pressure diffusion and in situ stress redistribution. Prior research on rocks and synthetic geomaterials consistently shows that higher injection rates lead to higher and sharper breakdown pressure curves, while lower rates promote greater fluid leak-off and delayed fracture initiation (Fallahzadeh et al. 2017; Zhou et al. 2016). Subsequent experimental works demonstrated that fluid penetration and pressurisation rate critically influence the timing and magnitude of breakdown pressure. At slow injection rates, hydraulic diffusion into the rock matrix delays fracture initiation, whereas at higher rates, the process becomes undrained and governed by tensile strength (Arzuaga-Garcia & Einstein 2020; Uwaifo 2016). Numerical studies highlight that the balance between injection rate and matrix permeability controls the transition between leak-off-dominated and hydraulically dominated regimes (Ulven & Sun 2018). Collectively, these findings emphasise that flow rate is

not a neutral experimental variable but a critical factor that must be standardised when applying hydraulic-fracturing-based strength tests.

Despite CPB's typically high porosity, evolving permeability, and fluid sensitivity – properties that are strongly dependent on mix design, solids concentration, and achieved density – no systematic studies have quantified how injection flow rate affects FIP. Previous CPB investigations have validated FIP as a strength indicator under fixed conditions, but the dependence of FIP on flow rate remains undocumented. This knowledge gap motivates the present work, which evaluates how injection flow rate influences fracture initiation in CPB and identifies conditions where rate effects become negligible.

1.2 Objective and scope of the study

The present study investigates how injection flow rate influences the FIP during hydraulic fracturing tests on CPB. Using AW32 hydraulic oil as the fracturing fluid, cylindrical CPB specimens were tested at controlled flow rates ranging from 1 to 50 mL/min to examine how the rate of pressurisation governs fracture initiation behaviour. Establishing such operational thresholds is essential for future field implementation of this testing method, ensuring that measured FIP values accurately represent the intrinsic tensile strength of the backfill rather than experimental artifacts. The outcomes of this study are interpreted to quantify the relationship between flow rate and FIP under controlled laboratory conditions and to develop practical recommendations for selecting optimal injection rates in hydraulic fracturing tests. These findings contribute to advancing hydraulic fracturing as a reliable technique for in situ strength evaluation of CPB, supporting safer and more predictable ground control in underground mining operations.

2 Methodology

The experimental program was designed to evaluate the influence of injection flow rate on FIP in CPB under controlled laboratory conditions. Cylindrical CPB specimens were prepared and cured for 28 days before being subjected to a series of hydraulic fracturing tests conducted at different flow rates. The measured FIP values were benchmarked against conventional mechanical tests, including UCS, BTS, and K_{Ic}, to ensure consistency and comparative reliability. Each test type was performed on 5 replicate samples to minimise variability and establish statistical confidence. A schematic overview of the experimental workflow is presented in Figure 1, outlining the sequential stages of sample preparation, curing, and testing adopted in this study.

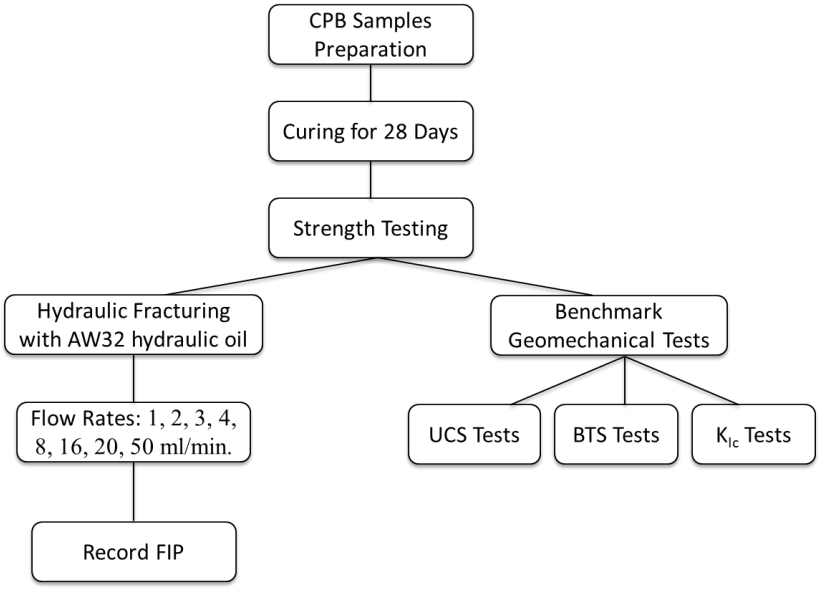

Figure 1 A schematic overview of the experimental plan followed in the proposed research. CPB = cemented paste backfill, FIP = fracture initiation pressure, UCS = uniaxial compressive strength, BTS = Brazilian tensile strength, K_{Ic} = Mode-I fracture toughness

2.1 C mix preparation

The CPB samples were produced using silica fine tailings (Sil-Co-Sil 52) which is a high-purity, inert ground silica powder with a median particle size around 52 µm, Type I Portland cement, and tap water. The silica tailings particle size distribution, as shown in Figure 2, represents that of typical underground mine tailings (Sivakugan et al. 2015). The mixture was formulated with a solids content of 75% by weight and a binder content of 8% by weight of total solids. Although detailed rheological parameters such as yield stress and slump were not measured in this study, the chosen solids content and binder content fall within the typical operating ranges reported for CPB (Ercikdi et al. 2014; Klein & Simon 2006; Landriault 1995). All materials were mixed in a Hobart mechanical mixer for 15 minutes at a constant speed to achieve uniform slurry consistency and complete dispersion of the cementitious binder. After mixing, the paste was cast into moulds of various geometries tailored to the specific testing requirements. Cylindrical moulds measuring 2″ by 4″ were used for both hydraulic fracturing and UCS tests, while 2″ diameter disc-shaped moulds were used for BTS and K_{Ic} tests. All samples were sealed immediately after casting to minimise moisture loss and cured at room temperature for a period of 28 days. To ensure consistent hydration conditions, the specimens were maintained in a fog-room environment, which provided a high-humidity atmosphere and prevented drying shrinkage throughout the curing period. The particle size distribution of the Sil-co-sil 52 silica fines is shown in Figure 2.

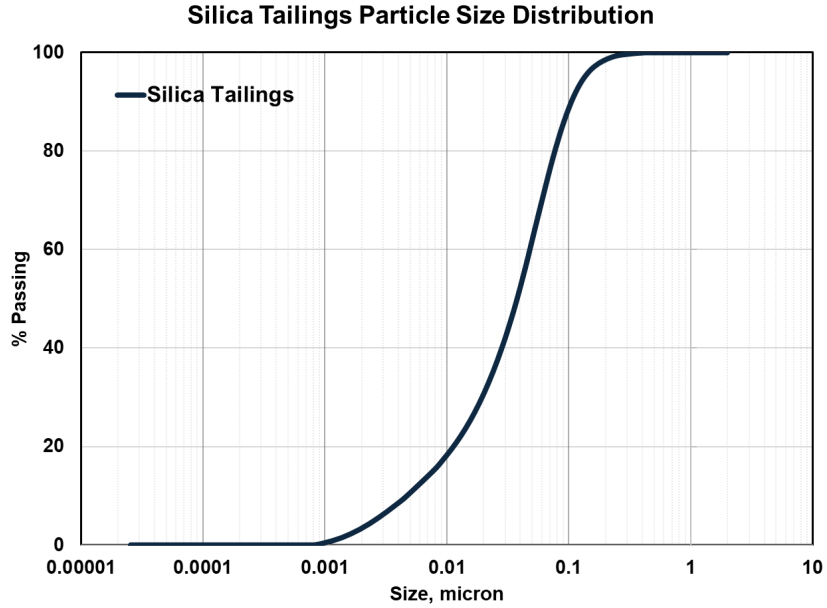

Figure 2 Particle size distribution of the silica tailings used in cemented paste backfill preparation

2.2 Hydraulic fracturing test

A custom fracture initiation system developed by Frimpong et al. (2025) was employed to perform hydraulic injection tests on the CPB samples. As illustrated in Figure 3a, the setup consisted of a flow-controlled syringe pump connected to a high-precision pressure transducer for real-time pressure monitoring. The pressure transducer had a maximum operating capacity of 3,000 psi with a full-scale error of ±0.2%, ensuring accurate measurement throughout the experiment. The syringe pump was capable of delivering a constant flow rate of fracturing fluid; in this study, AW32 hydraulic oil. The test specimens were 2″ × 4″ cylindrical samples (Figure 3B). A 1/8″ diameter stainless steel injection tube served as the fracturing conduit. Prior to testing, a 1/8″ diameter hole was drilled through the centre of each specimen to a depth of 2.25″, after which the injection tube was inserted to a depth of 2.0″, leaving a 0.25″ open section at the borehole base to allow pressure buildup and fracture initiation. A 1/4″ diameter counterbore, approximately 0.5″ deep, was then drilled at the top of the hole to provide a recess for sealing. The tube was secured using quick-setting, high-strength epoxy, ensuring proper alignment and a leak-tight connection. During each test, the syringe pump injected AW32 hydraulic oil at constant flow rates of 1, 2, 3, 4, 8, 16, 20, and 50 ml/min, resulting in an

increase in pressure within the specimen. The pressure continued to rise until reaching a peak value, defined as the FIP, at which point the sample fractured and the pressure dropped sharply, marking the onset of hydraulic fracturing within the CPB. A schematic overview of the hydraulic fracture initiation setup and the geometry of the CPB specimen used in the tests are presented in Figure 3.

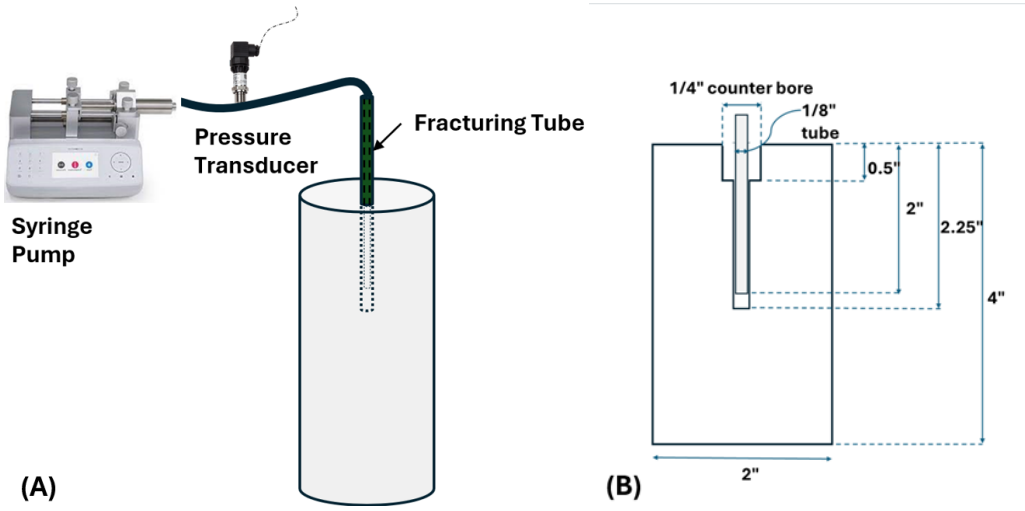

Figure 3 (a) Schematic of the fracture initiation setup showing the syringe pump, pressure transducer, and data acquisition system; (b) Dimensions of the cemented paste backfill sample and central borehole used for hydraulic fracturing tests

2.3 Benchmark strength tests

The mechanical strength of the CPB was evaluated using three standard benchmark tests: UCS, BTS and K_{Ic}. The UCS tests were performed in accordance with ASTM C39/C39M-21 (ASTM International 2023) using an INSTRON 5982 testing machine with a 22-kip load capacity. Each specimen was loaded under displacement control at a rate of 1 mm/min until failure, and the maximum load prior to failure was used to calculate the UCS. The BTS tests followed ASTM C496/C496M-17 (ASTM International 2017) and were conducted on disc-shaped CPB samples using the same testing machine. The discs were loaded diametrically at a constant rate of 0.2 mm/min until splitting failure occurred. The BTS was determined from the maximum recorded load and specimen geometry. Fracture toughness, K_{Ic}, was determined using the semi-circular bend (SCB) method developed by Chong & Kuruppu (1984). Semi-circular CPB specimens containing a 0.5" vertical notch were loaded at a constant rate of 0.2 mm/min until fracture, K_{Ic} was computed based on the recorded peak load and the sample dimensions.

3 Results and analysis

3.1 Mechanical characterisation of cemented paste backfill

Prior to fracturing, the CPB samples were subjected to UCS, BTS and K_{Ic} following established standards. These standardised mechanical tests were performed on samples prepared from the same mixing and curing batch as those used in the hydraulic fracturing experiments to establish reference strength parameters for the CPB. The resulting mean values and standard deviations are summarised in Table 1. The average UCS of 260 psi, BTS of 63 psi, and K_{Ic} of 40 psi√in fall within the expected range for CPB samples containing 8% binder and cured for 28 days, as reported previously (Frimpong et al. 2025). This alignment validates the consistency of the current material system with previously characterised CPB matrices. The low standard deviations (±10 psi for UCS, ±4 psi for BTS, ±2 psi√in for K_{Ic}) reflect good material uniformity across the test series.

Table 1 Benchmark mechanical properties of the cemented paste backfill

Property	Mean value	Standard deviation	Test method
UCS	260 psi	±10 psi	ASTM C39/C39M-21
BTS	63 psi	±4 psi	ASTM C496/C496M-17
K_{Ic}	40 psi√in	±2 psi√in	Semi-circular bend

UCS = uniaxial compressive strength, BTS = Brazilian tensile strength, KIc = Mode-I fracture toughness

3.2 Fracture initiation pressure measurements

FIP was determined for each hydraulic fracturing test as the maximum borehole pressure recorded immediately prior to the abrupt post-peak decline, signifying the onset of tensile crack propagation from the borehole wall. This parameter was extracted from pressure–time curves acquired after each test. The use of AW32 low-viscosity hydraulic oil, with a viscosity of 26 cSt, ensured consistent fluid properties across all tests. A total of 40 fracturing tests (5 replicates per flow rate) were conducted on independently prepared CPB cylinders, all sourced from the same batch to minimise inter-batch variability in silica tailings mineralogy, binder hydration kinetics, and initial porosity. The compiled FIP data are presented in Table 2, which reports mean values alongside standard deviations calculated from the five replicates at each flow rate.

Table 2 Mean fracture initiation pressure (FIP) values at varying injection flow rates

Flow rate (ml/min)	FIP (psi)	Standard deviation (psi)
1	403.1	(±28.3)
2	473.4	(±9.7)
3	475.8	(±14.0)
4	484.7	(±28.2)
8	532.1	(±45.5)
16	557.2	(±47.5)
20	576.6	(±13.5)
50	568.4	(±29.2)

The mean FIP increases steadily from approximately 403 psi at 1 ml/min to 532 psi at 8 ml/min, representing an overall increase of about 32%. Beyond 8 ml/min, the pressure tends to plateau, fluctuating between 560–580 psi. This non-monotonic trend underscores a transition in governing mechanisms: at flow rates ≤8 ml/min, FIP is appreciably sensitive to injection rate, delaying the onset of fracture. Conversely, at flow rates ≥8 ml/min, FIP approaches a quasi-asymptotic regime, where further rate increase yields diminishing returns, and observed values are predominantly dictated by the inherent tensile resistance of the CPB. Standard deviations ranged from ±9.7 to ±47.5 psi. This variation reflects the inherent heterogeneity of CPB, including local variations in pore structure, particle packing, and binder hydration within nominally identical specimens. The FIP–flow rate relationship is graphically depicted in Figure 4, with mean data points and error bars representing ±1 standard deviation from the mean. The plot describes two distinct behavioural domains: a rate-dependent regime (1–8 ml/min) characterised by a steep positive slope, and a rate-insensitive plateau (>8 ml/min) with near-constant FIP. This inflection near 8 ml/min establishes the threshold beyond which the effects of flow rate dependence of FIP are negligible relative to the timescale of pressurisation. For other tailings and binder recipes, the exact inflection point may shift and should be verified experimentally, but our results indicate that selecting injection rates well above the transition (e.g. in the range of 16–50 mL/min for

laboratory-scale specimens) provides a practical way to ensure that testing is conducted within the plateau, strength-controlled regime.

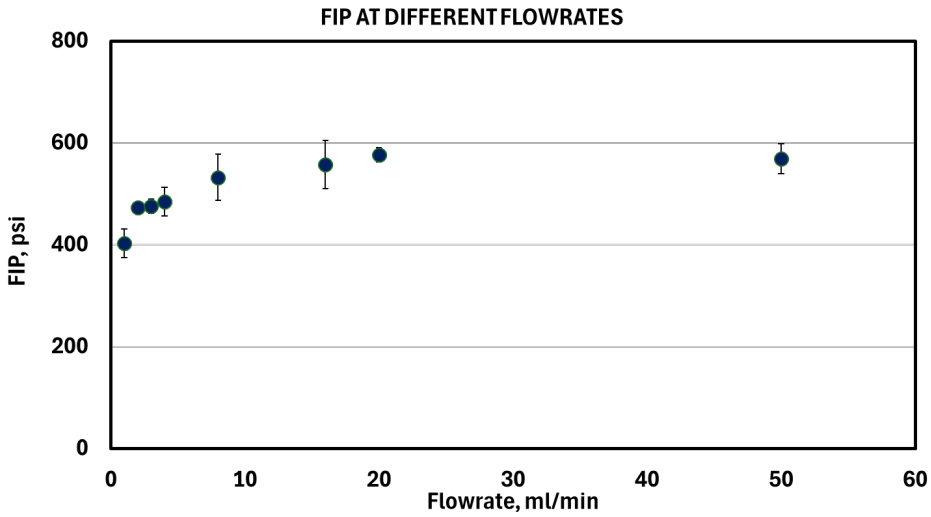

Figure 4 Variation of fracture initiation pressure (FIP) with injection flow rate for AW32 hydraulic oil

3.3 Pressure–time response curves

Continuous pressure–time curves were acquired throughout each hydraulic fracturing test to interpret the dynamic pressurisation behaviour and leak-off characteristics of the CPB under varying injection flow rates. Representative pressure–time curves for all 8 flow rates are presented in Figure 5. Each curve corresponds to a single replicate selected for its proximity to the mean FIP at that flow rate, thereby illustrating typical behavioural patterns while preserving reliability to the collective statistics reported in Section 3.2. All curves exhibit the same fundamental structure but with distinct differences in slope, peak magnitude, and time to fracture initiation as the flow rate increases.

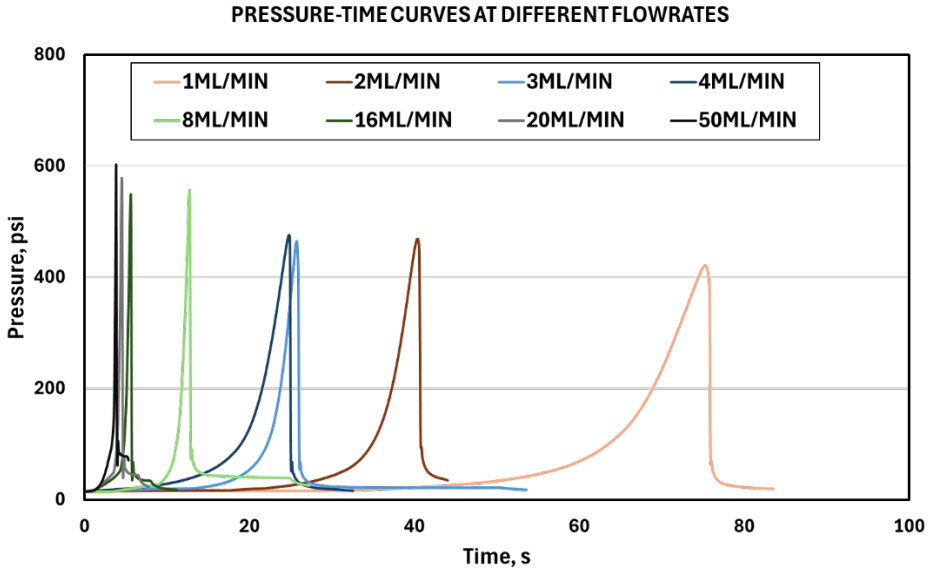

Figure 5 Representative pressure–time curves at different flow rates

3.3.1 General shape of the pressure–time curves

Across all flow rates, the pressure–time response exhibited three distinct phases that collectively characterise the hydraulic fracture initiation process. During the initial stage, the pressure rose linearly with time as the borehole cavity was filled with the incompressible AW32 oil. In this region, the CPB matrix responded elastically to the gradually increasing internal pressure, resulting in a linear slope whose steepness directly reflected the imposed flow rate. The absence of deviation from linearity indicates that the material remained intact, with no significant microcracking or fluid infiltration beyond the borehole wall.

As the pressure approached the tensile limit of the CPB, the curves began to deviate from linearity, marking the second stage of the process. This deviation indicates the onset of localised microcracking and pore dilation near the borehole wall. Energy input during this stage is partly dissipated through microcrack growth rather than stored elastically, causing the curve to bend gradually toward a peak. The magnitude and duration of this transition zone varied with flow rate, subtle and extended under low injection rates but sharper and shorter under high rates, indicating that faster pressurisation accelerates the accumulation of stress and limits time-dependent relaxation.

The third and final stage corresponds to the fracture initiation event itself. Once the internal fluid pressure exceeded the tensile capacity of the CPB, a sudden tensile fracture propagated radially outward from the borehole, producing an abrupt pressure drop. This drop represents the instantaneous release of stored elastic energy and the rapid expansion of fluid volume into the new fracture space. At higher flow rates, the pressure fall was sharp and almost instantaneous, whereas at lower rates, it was more gradual due to partial leak-off and slower crack opening. The single, clean peak followed by a distinct pressure drop in all curves confirms that each test produced a single, dominant fracture event with no secondary re-opening or branching.

3.3.2 Effect of flow rate on curve characteristics

The influence of flow rate on the evolution of pressure with time was pronounced and systematic as shown in Figure 5. At the lowest flow rate of 1 ml/min, the pressure increased slowly and almost linearly for approximately 80 s before reaching fracture initiation. The gradual slope and long duration indicate slow borehole pressurisation, allowing time for partial fluid diffusion into the pore network of the CPB and, consequently, a delayed buildup of tensile stress at the borehole wall. At 2 ml/min, the time to FIP reduced to around 60 s, while at 3 mL/min, fracture occurred after roughly 25 s, demonstrating the progressive acceleration of stress accumulation with increasing injection rate.

When the flow rate increased to 4 ml/min, fracture initiation occurred at about 22 s, and the slope of the pressurisation segment became noticeably steeper. The non-linearity preceding the peak also became more pronounced, reflecting more rapid microcrack development and reduced leak-off time. At 8 mL/min, the pressure rose sharply, reaching its maximum after only 12 s. This marked the transition between leak-off-influenced and hydraulically dominated pressurisation, where the rate of injection began to exceed the material's capacity for fluid diffusion.

At higher flow rates, 16, 20, and 50 ml/min, the pressure–time response was characterised by extremely steep, almost instantaneous rises to peak values occurring within approximately 5, 4, and 3 s, respectively. The nearly vertical slopes and abrupt post-peak drop in these curves indicate that the borehole and surrounding CPB behaved as an almost undrained system, with negligible fluid penetration before fracture. In this regime, the fracture initiation pressure is governed primarily by the tensile strength of the CPB rather than by hydraulic diffusion effects.

These flow rate-dependent trends are consistent with findings reported in previous hydraulic fracturing studies on geomaterials. Fallahzadeh et al. (2017) observed that higher injection rates in synthetic mortar samples led to steeper pressure–time curves and higher breakdown pressures, attributing this to increased fracturing energy and reduced leak-off. Similarly, Zhou et al. (2016) used a coupled fluid-mechanical numerical framework, and showed that higher injection rates shortened the time to fracture and elevated peak pressure due to undrained loading conditions.

4 Discussion

4.1 Characteristic distance and the point stress model

The relationship between FIP and the tensile failure of brittle geomaterials has traditionally been explained using linear–elastic (LE) or thick-walled pressure-vessel models. However, as demonstrated in our earlier work (Frimpong et al. 2025), these classical models significantly overpredict the tensile strength of CPB, primarily because they neglect the scale-dependent redistribution of stress that occurs around small boreholes. To address this limitation, the point stress (PS) model, originally introduced by Whitney & Nuismer (1974) and adapted for hydraulic fracturing by Ito & Hayashi (1991) was applied. The PS model provides a physically interpretable link between the FIP and the material's inherent fracture properties through a characteristic distance, d. This model has been validated by comparing predicted tensile strengths from the model with measured BTS for CPB samples of different binder contents (Frimpong et al. 2025). The model successfully corrected the overprediction seen in LE approaches and produced a consistent relationship between FIP and tensile strength. The present study extends that application by exploring how d evolves dynamically with flow rate, providing a mechanistic insight for why low-rate injections yield varying FIP values, while high-rate injections reflect nearly consistent FIP values. The subsequent sections interpret these 2 regimes in detail.

The central premise of the model is that a pressurised borehole in a brittle medium fails not when the stress at the borehole wall equals the tensile strength, but when the average tensile stress over a finite distance, d, ahead of the wall reaches the tensile strength. This characteristic distance represents the effective zone of stress redistribution and microcrack interaction and is therefore a material property related to its tensile strength and fracture toughness. According to the model, the characteristic distance can be computed from the material's tensile strength and mode-I fracture toughness K_{Ic} using the expression derived by Ito & Hayashi (1991) (Equation 1):

$$d = \frac{1}{2\pi}\left(\frac{K_{Ic}}{\sigma_T}\right)^2 \tag{1}$$

where:

K_{Ic} = the material's fracture toughness

σ_T = the material's tensile strength.

Once d is known, it can be coupled with the geometric correction factor I, which accounts for borehole size effects through the ratio of the borehole radius to the characteristic distance (Equation 2):

$$I = \frac{r_i}{r_i + d} \tag{2}$$

where r_i is the borehole radius.

The corresponding FIP is then obtained as Equation 3:

$$FIP = \frac{\sigma_T}{I^2} \tag{3}$$

These 3 relationships form the analytical basis of the PS model. In the current study, the model was employed in reverse to investigate how the characteristic distance d evolves with injection flow rate, thereby linking hydraulic behaviour to the underlying fracture mechanics of CPB. Using the measured FIP values at each flow rate, the geometric term I was first computed from Equation 4:

$$I = \sqrt{\frac{FIP}{\sigma_T}} \tag{4}$$

This was subsequently used in Equation 2 to back-calculate the corresponding characteristic distance d for each flow rate. The calculated values of d are presented in Figure 6, which plots the evolution of characteristic

distance with flow rate. The results show that d increases sharply from low to moderate flow rates (1–8 ml/min), then levels off beyond 8 ml/min, mimicking the trends in FIP.

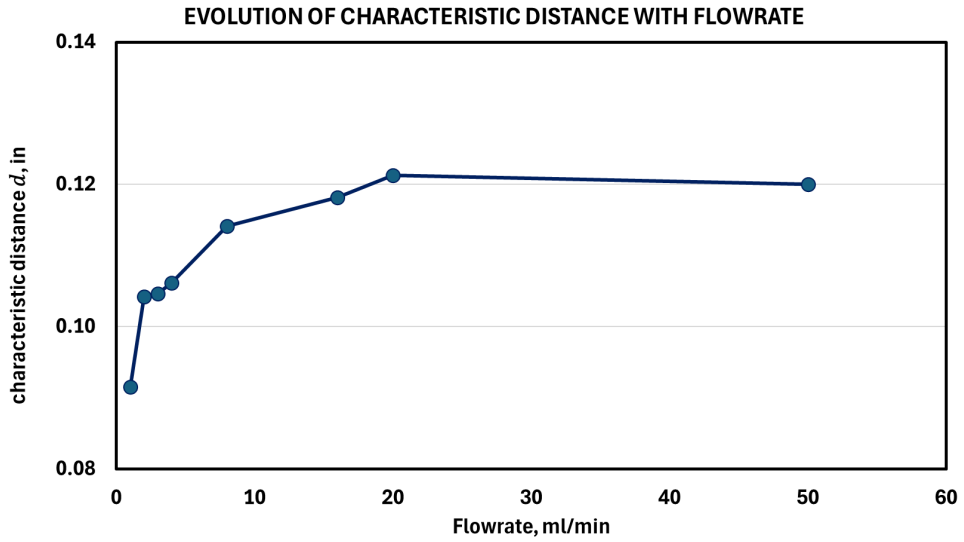

Figure 6 Variation of characteristic distance d with injection flow rate

4.1.1 Low-flow rate regime

At low injection flow rates, the pressure–time responses display gradual pressurisation slopes and broad peaks, corresponding to slower stress buildup and significant hydraulic leak-off. The injected oil penetrates the pore structure of the CPB before the pressure field fully develops, allowing local pore dilation and microcrack nucleation near the borehole wall. This results in delayed fracture initiation and lower FIP values, as described in Section 3.3. From the perspective of the PS model, this regime is characterised by a progressively increasing characteristic distance (d) with flow rate (Figure 6). At the lowest rates (1–4 ml/min), d values between 0.09 and - 0.11 in indicate that only a small volume of material surrounding the borehole contributes to the fracture process. The stress concentration remains highly localised, and part of the injected energy dissipates through seepage and pore-fluid diffusion rather than stored elastically. This explains both the elongated time-to-peak in the pressure–time curves (60–80 s) and the FIP rise over this interval.

As the rate increases toward 8 ml/min, the leak-off timescale becomes comparable to the pressurisation timescale, and the effective zone of stress redistribution widens. The corresponding increase in d to about 0.11 in reflects this expansion of the stress influence zone, meaning that a larger fraction of the CPB matrix is elastically engaged before failure. This coupled hydraulic–mechanical interaction produces the smooth, rounded peaks observed in the pressure–time curves, where the energy is partitioned between fluid infiltration and gradual tensile crack coalescence. The model thus explains the delayed and diffused failure signatures: fracture initiation occurs once the averaged tensile stress across the evolving d zone reaches the material's intrinsic strength, rather than instantaneously at the borehole wall. In this regime, both the FIP and d are rate-dependent, indicating that the hydraulic process, in addition to the material strength, controls the initiation pressure. Consequently, FIP values obtained below 8 ml/min represent diffusion-controlled fracture rather than true material strength.

4.1.2 High-flow rate regime

Beyond 8 ml/min, both the FIP and the characteristic distance d reach asymptotic values around 570 psi and 0.12 in, respectively. This indicates that the fracturing process transitions to a rate-insensitive, strength-controlled regime. In this range, the time required to pressurise the borehole becomes much shorter than the time required for fluid to diffuse through the pore network. The CPB therefore behaves as an undrained medium, and nearly all injected energy is stored elastically within the matrix until tensile failure occurs. The corresponding pressure–time curves at these rates show sharp, nearly vertical rises to peak

pressure (within 3–5 s), followed by abrupt post-peak drops, signatures of a single, dominant fracture event with minimal leak-off.

Within the PS model framework, the consistency of d signifies that the stress redistribution zone has reached a stable, intrinsic value. Once pressurisation exceeds the leak-off capacity of the matrix, the borehole begins to mobilise a fixed representative volume of material, leading to consistent and repeatable failure of the CPB. The stabilisation of the characteristic distance explains the observed plateau in FIP, as d becomes constant, Equation 4 predicts no further increase in FIP with flow rate. This transition indicates fracturing occurs through bulk tensile failure of the backfill.

This behaviour is also consistent with the steep, narrow peaks in the pressure–time curves observed at 16–50 ml/min. The near-instantaneous pressurisation ensures that the effective tensile stress distribution remains uniform across the stable d zone, causing fracture initiation to occur as soon as the average stress equals σ_T. Because both d and FIP remain constant, this regime defines the operational threshold for reliable FIP-based strength evaluation. Tests performed above 8 ml/min yield consistent results that reflect the true tensile capacity of the CPB, uninfluenced by hydraulic diffusion effects.

4.2 Mechanistic interpretation

The complementary trends of FIP and characteristic distance d demonstrate that fracture initiation in CPB is governed by a transition from a diffusion-controlled to a strength-controlled failure mechanism. At low flow rates, slow pressurisation allows fluid leak-off and partial pore pressure equilibration, restricting tensile stress to a small zone around the borehole. The increasing d values with flow rate capture the progressive expansion of this stressed volume as leak-off effects diminish. Once the injection rate exceeds approximately 8 mL/min, both FIP and d reach steady-state values, indicating that the pressurisation process has become undrained and that the fracture initiation mechanism is dictated primarily by the intrinsic tensile strength of the CPB.

From the standpoint of the PS model, this stabilisation of d signifies that the near-borehole stress redistribution has reached a physically characteristic scale of the material. In this condition, the average tensile stress over the distance d equals the material's tensile strength and further increases in flow rate do not alter the stress field geometry. This interpretation explains why the measured FIP values converge toward an asymptotic limit and why the pressure–time curves evolve from broad, diffusion-dominated peaks to sharp, instantaneous drops. The correspondence between the constant d and the constant FIP therefore reflects a unified mechanical response where the hydraulic and tensile components of failure are fully coupled. Mechanistically, the constant d at high flow rates implies that the volume of material participating in fracture initiation is both maximised and repeatable. The resulting FIP therefore represents a bulk property rather than a local measurement influenced by pore connectivity or transient seepage.

5 Conclusion

This study investigated the effect of injection flow rate on FIP in CPB and introduced a mechanistic interpretation using the PS model. The main findings are as follows:

1. Flow rate controls both hydraulic response and failure mechanism: the measured FIP increased at 1 to 8 ml/min and then plateaued, indicating a transition from a leak-off-dominated to a strength-controlled regime. Corresponding pressure–time curves changed from broad, diffusion-governed peaks at low rates to sharp, instantaneous fracture events at higher rates.
2. Fracture initiation in CPB follows 2 distinct regimes: in the low-flow rate regime (≤ 8 ml/min), fracture initiation is diffusion-controlled; fluid leak-off and local pore dilation delay tensile failure, producing variable d and variable FIP values. In the high-flow rate regime (≥ 8 ml/min), the system behaves as undrained; the stress field becomes uniform, d remains constant, and FIP reflects the intrinsic tensile strength of the backfill.

3. Practical implication for strength evaluation: reliable and repeatable FIP-based strength measurements of CPB require operating in the high-flow rate regime. Injection flow rates of 8 mL/min or higher are recommended to minimise hydraulic diffusion effects and ensure that the measured FIP corresponds to the material's true tensile capacity.
4. Broader significance and future work: the combined use of hydraulic fracturing tests and the PS model provides a physically grounded framework for linking injection dynamics, fracture mechanics, and backfill strength. To extend its applicability, future research will:
    a. extend the present laboratory program to CPB formulated with field derived mine tailings from mine operations, in order to demonstrate the robustness of the technique
    b. perform field-scale hydraulic fracturing tests to validate the observed flow rate dependence under in situ conditions
    c. systematically investigate the influence of fluid viscosity on fracture initiation behaviour and the evolution of d.
5. These efforts will help establish a comprehensive understanding of fluid-driven fracture mechanisms in CPB and enhance the practical deployment of this method for real-time strength assessment in underground mines.

References

Aref, K 1988, *A Study of the Geotechnical Characteristics and Liquefaction Potential of Paste Backfill*, PhD thesis, McGill University, Montreal.

Arzuaga-Garcia, I & Einstein, H 2020, 'Experimental study of fluid penetration and opening geometry during hydraulic fracturing', *Engineering Fracture Mechanics*, vol. 230, p. 106986.

ASTM International 2017, *Standard Test Method for Splitting Tensile Strength of Cylindrical Concrete Specimens (ASTM C496/C496M-17)*, ASTM International, West Conshohocken.

ASTM International 2023, *Standard Test Method for Compressive Strength of Cylindrical Concrete Specimens (ASTM C39/C39M-21)*, ASTM International, West Conshohocken.

Been, K, Brown, ET & Hepworth, N 2002, 'Liquefaction potential of paste fill at Neves Corvo mine, Portugal', *Transactions of the Institution of Mining and Metallurgy Section A – Mining Technology*, vol. 111, pp. A47–A58.

Chen, G, Ye, Y, Yao, N, Fu, F, Hu, N & Zhang, Z 2022, 'Deformation failure and acoustic emission characteristics of continuous graded waste rock cemented backfill under uniaxial compression', *Environmental Science and Pollution Research*, vol. 29, no. 53, pp. 80109–80122, https://doi.org/10.1007/s11356-022-23394-x

Chong, KP & Kuruppu, MD 1984, 'New specimen for fracture-toughness determination for rock and other materials', *International Journal of Fracture*, vol. 26, no. 2, pp. R59–R62, https://doi.org/10.1007/BF01157555

Ercikdi, B, Yılmaz, T & Külekci, G 2014, 'Strength and ultrasonic properties of cemented paste backfill', *Ultrasonics*, vol. 54, no. 1, pp. 195–204.

Fallahzadeh, SH, Hossain, MM, James Cornwell, A & Rasouli, V 2017, 'Near wellbore hydraulic fracture propagation from perforations in tight rocks: the roles of fracturing fluid viscosity and injection rate', *Energies*, vol. 10, no. 3, p. 359.

Frimpong, J & Pandey, R 2025, 'Novel hydraulic measurement technique to enable reliable strength evaluation of cemented paste backfill in underground mines', *Proceedings of the 59th US Rock Mechanics/Geomechanics Symposium*, American Rock Mechanics Association, Alexandria.

Frimpong, JA, Shabab, BA, Pandey, R, Chatterjee, S, Walton, G & Brand, AS 2025, 'Fracture initiation pressure as a measure of cemented paste backfill strength', *Mining, Metallurgy & Exploration*, vol. 42, no. 3, pp. 1305–1323, https://doi.org/10.1007/s42461-025-01257-6

Haimson, B & Fairhurst, C 1967, 'Initiation and extension of hydraulic fractures in rocks', *Society of Petroleum Engineers Journal*, vol. 7, no. 3, pp. 310–318.

Haimson, B & Fairhurst, C 1969, 'Hydraulic fracturing in porous-permeable materials', *Journal of Petroleum Technology*, vol. 21, no. 7, pp. 811–817.

Helinski, M 2007, *Mechanics of Mine Backfill*, PhD thesis, The University of Western Australia, Perth.

Hubbert, MK & Willis, DG 1957, 'Mechanics of hydraulic fracturing', *Transactions of the American Institute of Mining and Metallurgical Engineers*, vol. 210, no. 6, pp. 153–163.

Ito, T & Hayashi, K 1991, 'Physical background to the breakdown pressure in hydraulic fracturing tectonic stress measurements', *International Journal of Rock Mechanics and Mining Sciences & Geomechanics Abstracts*, vol. 28, no. 4, pp. 285–293.

Johnson, JC, Seymour, JB, Martin, LA, Stepan, M & Akroosh, A 2015, 'Strength and elastic properties of paste backfill at the Lucky Friday mine, Mullan, Idaho', *Proceedings of the 49th US Rock Mechanics/Geomechanics Symposium*, American Rock Mechanics Association, Alexandria.

Kesimal, A, Yilmaz, E, Ercikdi, B, Alp, I & Deveci, H 2005, 'Effect of properties of tailings and binder on the short- and long-term strength and stability of cemented paste backfill', *Materials Letters*, vol. 59, no. 28, pp. 3703–3709.

Klein, K & Simon, D 2006, 'Effect of specimen composition on the strength development in cemented paste backfill', *Canadian Geotechnical Journal*, vol. 43, no. 3, pp. 310–324.

Landriault, D 1995, 'Paste backfill mix design for Canadian underground hard rock mining', *Proceedings of the 12th Mine Operators Conference*, Canadian Institute of Mining, Westmount.

Le Roux, K, Bawden, WF & Grabinsky, MF 2002, 'Comparison of the material properties of in situ and laboratory prepared cemented paste backfill', *Proceedings of the CIM Conference*, Canadian Institute of Mining, Westmount.

Le Roux, K, Bawden, WF & Grabinsky, MF 2005, 'Field properties of cemented paste backfill at the Golden Giant mine', *Transactions of the Institutions of Mining and Metallurgy Section A – Mining Technology*, vol. 114, no. 2, pp. A65–A80, https://doi.org/10.1179/037178405X44557

Li, D, Liu, B, He, J, Li, X & Jian, M 2017, 'Strength and transportability of cemented phosphogypsum paste backfilling slurry', in A Wu & R Jewell (eds), *Paste 2017: Proceedings of the 20th International Seminar on Paste and Thickened Tailings*, University of Science and Technology Beijing, Beijing, pp. 328–336, https://doi.org/10.36487/ACG_rep/1752_36_Li

Mitchell, RJ 1991, 'Sill mat evaluation using centrifuge models', *Mining Science and Technology*, vol. 13, pp. 301–313.

Qiu, H, Zhang, F, Liu, L, Hou, D & Tu, B 2020, 'Influencing factors on strength of waste rock tailing cemented backfill', *Geofluids*, vol. 2020, article 8847623.

Sheshpari, M 2015, 'A review of underground mine backfilling methods with emphasis on cemented paste backfill', *Electronic Journal of Geotechnical Engineering*, vol. 20, no. 13, pp. 5183–5208.

Sivakugan, N, Veenstra, R & Naguleswaran, N 2015, 'Underground mine backfilling in Australia using paste fills and hydraulic fills', *International Journal of Geosynthetics and Ground Engineering*, vol. 1, article 1.

Stone, D 2021, 'Paste quality control benchmarks', *MineFill 2020–2021: Proceedings of the 13th International Symposium on Mining with Backfill*, pp. 35–43.

Ulven, OI & Sun, W 2018, 'Capturing the two-way hydromechanical coupling effect on fluid-driven fracture in a dual-graph lattice beam model', *International Journal for Numerical and Analytical Methods in Geomechanics*, vol. 42, no. 5, pp. 736–767.

Uwaifo, E 2016, *Time-dependent Initiation of Multiple Hydraulic Fractures in Rocks*, PhD thesis, University of Pittsburgh, Pittsburgh.

Wang, F, Zheng, Q, Zhang, G, Wang, C, Cheng, FQ & Geng, L 2020, 'Preparation and hydration mechanism of mine cemented paste backfill material for secondary smelting water-granulated nickel slag', *Journal of New Materials for Electrochemical Systems*, vol. 23, no. 1, pp. 51–59, https://doi.org/10.14447/jnmes.v23i1.a10

Whitney, JM & Nuismer, RJ 1974, 'Stress fracture criteria for laminated composites containing stress concentrations', *Journal of Composite Materials*, vol. 8, no. 3, pp. 253–265.

Xin, L 2021, 'Meso-scale modeling of the influence of waste rock content on mechanical behaviour of cemented tailings backfill', *Construction and Building Materials*, vol. 307, p. 124473.

Yilmaz, E 2010, *Investigating the Hydrogeotechnical and Microstructural Properties of Cemented Paste Backfill Using the CUAPS Apparatus*, PhD thesis, Université du Québec en Abitibi-Témiscamingue, Rouyn-Noranda.

Yin, S, Shao, Y, Wu, A, Wang, H, Liu, X & Wang, Y 2020, 'A systematic review of paste technology in metal mines for cleaner production in China', *Journal of Cleaner Production*, vol. 247, 119590, https://doi.org/10.1016/j.jclepro.2019.119590

Yumlu, M & Guresci, M 2007, 'Paste backfill bulkhead monitoring – a case study from Inmet's Çayeli mine, Turkey', *Proceedings of the 9th International Symposium on Mining with Backfill*.

Zhou, J, Zhang, L, Braun, A & Han, Z 2016, 'Numerical modeling and investigation of fluid-driven fracture propagation in reservoirs based on a modified fluid-mechanically coupled model in two-dimensional particle flow code', *Energies*, vol. 9, no. 9, p. 699.